Simulation of the Magnetic Induction Vector of a Magnetic Core to be Used in FFC NMR Relaxometry

A. Roque · S. Ramos · J. Barão · M. Machado · D.M. Sousa · E. Margato · J. Maia

Abstract This paper is a contribution for the assessment and comparison of magnet properties based on magnetic field characteristics particularly concerning the magnetic induction uniformity in the air gaps. For this aim, a solver was developed and implemented to determine the magnetic field of a magnetic core to be used in Fast Field Cycling (FFC) Nuclear Magnetic Resonance (NMR) relaxometry. The electromagnetic field computation is based on a 2D finite-element method (FEM) using both the scalar and the vector potential formulation. Results for the magnetic field lines and the magnetic induction vector in the air gap are presented. The target magnetic induction is 0.2 T, which is a typical requirement of the FFC NMR technique, which can be achieved with a magnetic core based on permanent magnets or coils. In addition, this application requires high magnetic induction uniformity. To achieve this goal, a solution including superconducting pieces is analyzed. Results are compared with a different FEM program.

Keywords Magnetic core · Magnetic uniformity · Superconductors · Permanent magnet

1 Introduction

Magnetic circuits must present in general a specific design in accordance with the requirements of the application. Depending on the structure and dimensions of the magnetic cores (shape, air gaps, etc.), the distribution of the flux lines is important to guarantee the performance of the magnetic system. In addition, for some applications the uniformity of the magnetic induction is the parameter to be optimized, as for instance, for the magnet of a Fast Field Cycling (FFC) Nuclear Magnetic Resonance (NMR) relaxometer. In general, the air gap is the region where the flux uniformity should be very high [1–3].

Using this model illustrated in Fig. 1 with the requirements of high magnetic induction uniformity, the magnetic induction was analyzed considering the following configurations: magnetic core with permanent magnets; magnetic core with coils; and, magnetic core with coils and superconducting pieces.

To analyze and compare these solutions, a *solver* to determine the magnetic field lines and the magnetic induction vector in their air gaps was developed and implemented. For each configuration, the models used to implement the computational routines were described and presented.

This work also includes the comparison of the results obtained with the developed *solver* with the ones obtained with a well-known finite-element method software [4].

The main properties of the superconducting materials are also described, bearing in mind the usage of such innovative superconducting materials, their electromagnetic characteristics and the dimensions of the core.

Fig. 1 Basic structure of the magnetic core

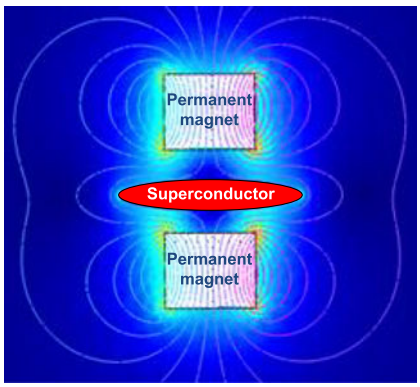

Fig. 2 Magnetic field lines of a system with permanent magnets and a superconductor

1.1 Effect of the Superconducting Pieces

As is well-known, the properties of superconducting materials are distinct from those of ordinary conducting materials.

By submitting some materials (Sn or Pb, for instance) to temperatures below their critical temperature and to a magnetic field, it can be observed that the flux lines do not cross the material. This phenomenon became known as the Meissner effect [5] and it is exemplified in Fig. 2 for the core where the induction magnetic field produced by two magnets is applied to a superconducting piece.

The behavior of a superconductor when exposed to the application of an external magnetic field leads to the following specific characteristics, typically, at very low temperatures, particularly when the temperature is below a critical temperature T_c:

- resistivity with temperature: $\rho = f(T)$;
- magnetization, $\vec{M} = f(\vec{H})$, and
- magnetic induction with the magnetic field, $\vec{B} = f(\vec{H})$.

The magnetic field, $\vec{H}$, the magnetic induction, $\vec{B}$, and magnetization, $\vec{M}$, are closely linked through the expression [6]

$$\vec{B} = \mu_0(\vec{H} + \vec{M}). \tag{1}$$

This expression is valid at any point, inside and outside of the material, knowing that outside of the material the magnetization may be taken zero, $\vec{M} = 0$.

In linear and isotropic materials, the magnetization is proportional to the applied magnetic field through the expression

$$\vec{M} = \chi_m \vec{H}, \tag{2}$$

where χ_m is the magnetic susceptibility of the material for the considered environment.

In this case, the magnetic induction is not nil and from (1) and (2) the following expressions are obtained:

$$\vec{B} = \mu_0(1 + \chi_m)\vec{H}, \tag{3}$$

$$\mu_r = 1 + \chi_m. \tag{4}$$

Moreover, if a superconductor is submitted to a magnetic field below a critical magnetic field (with a value depending on the superconducting material), the magnetic induction inside the superconductor is always null, $\vec{B} = 0$. This property may be given by (3) and (4) if susceptibility is taken as $\chi_m = -1$, which means that the relative magnetic permeability of the material is zero, $\mu_r = 0$. However, for computational reasons, a value of 0.005 for the relative magnetic permeability is taken inside YBCO superconductors for cases where this material is used in the real magnet [7].

2 Core with Permanent Magnets

The magnetic field in the magnetic core with permanent magnets (Fig. 3) is based on the scalar potential formulation.

Since the magnetic core is symmetrical, the calculations are performed considering only 1/4 of the magnet, as shown in Fig. 4.

2.1 Calculation of the Potential

The formulation of the problem for the regions without currents (free space) can be obtained using the scalar formulation [8]:

$$\nabla \cdot (\mu_r \nabla \phi) = 0, \tag{5}$$

where

$$\vec{H} = \vec{H}_S - \nabla \phi, \tag{6}$$

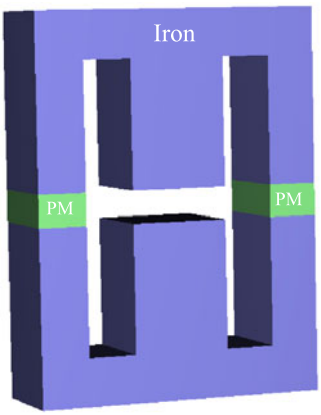

Fig. 3 Structure of the magnetic core with permanent magnets (PM)

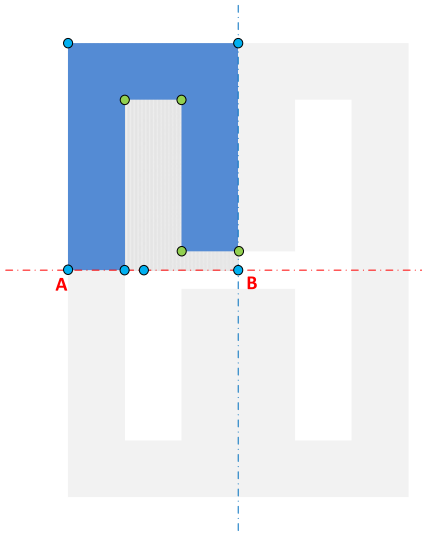

Fig. 4 Section of the magnetic core simulated

and $\vec{H}_S$ is assumed as the source magnetic field, since [9]:

$$\nabla \times \vec{H} = \nabla \times \vec{H}_S = \vec{J}_S, \tag{7}$$

where J_S is the current density.

Since the circuit is based on permanent magnets, $\vec{J}_S = 0$, so that

$$\nabla \times \vec{H} = 0, \quad \text{then} \tag{8}$$

$$\vec{H} = -\nabla\phi. \tag{9}$$

Using the finite-element method to solve (5), (10) and (11) are obtained [10]

$$\phi = \sum_{i=1}^{3} \phi_i (a_i + b_i x + d_i y), \tag{10}$$

where ϕ is the potential function approximation in a 2D first order triangular finite element.

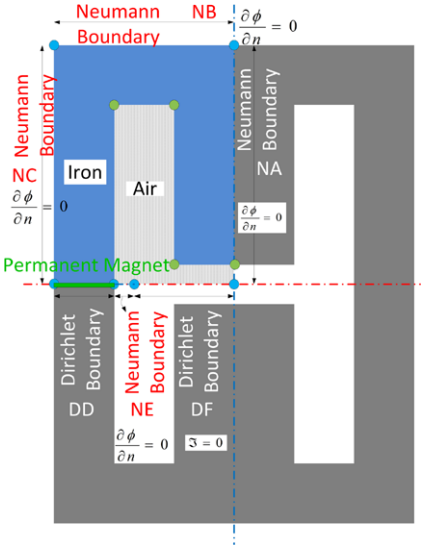

Fig. 5 Boundary conditions of the magnetic core with permanent magnets

So that the magnetic induction in the air is given by

$$\vec{B} = \mu_0 \left(-\sum_{i=1}^{3} \phi_i b_i \right) \vec{u}_x + \mu_0 \left(-\sum_{i=1}^{3} \phi_i d_i \right) \vec{u}_y, \tag{11}$$

where μ_0 is the vacuum magnetic permeability.

In the computational routine, the permanent magnet is implemented as shown in Fig. 5. The value of the source is equivalent to half of the number of turns of an existing real coil (320 turns) driven by a current of 5 A, being equivalent to a total magneto motive force (m.m.f.) of 800 AT.

At the first stage, when constructing the models, the different boundaries are connected in an anticlockwise direction, starting from an appropriate point.

Each point is defined by a pair of coordinates (x, y) and each boundary type is properly identified as Neumann or Dirichlet [10].

Due to the symmetry of the configuration, the Dirichlet boundary [DD] is represented by a source of value equal to 800 AT, as was explained previously.

After defining the coordinates of the points that bound the core, as well as its air gap, the definition and characterization of the boundary conditions, the type of material used and, finally, the value of the relative permeability of the various elements, a finite-element mesh generator is used to create the finite-element mesh according to the conditions mentioned above.

It is important to note that the Neumann boundary [NE] in Fig. 5 corresponds to the point where the equivalent source is applied imposing a m.m.f. equal to the potential difference between the two Dirichlet boundaries, the one crossing the iron (DD) and the other in the air gap (DF). Its size should be as small as possible in order to obtain

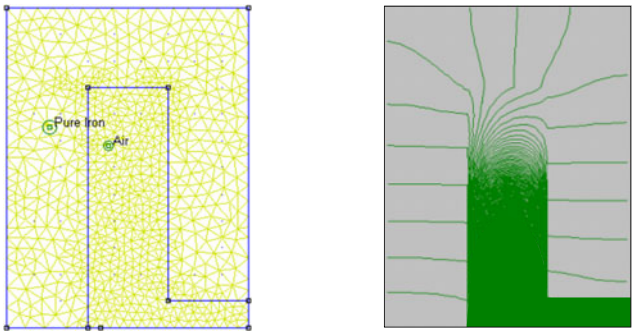

a) Mesh b) Equipotential lines

Fig. 6 Mesh and equipotential lines of the simulated section

the magnetic field configuration without significant perturbations.

Figure 6(a) represents the finite-element mesh that was created for this model (simulation based on the replacement of a permanent magnet by an equivalent source). As can be seen, the number of elements of the mesh can be established, in order to have more elements where the magnetic field is more important (greater values of the potential gradient) and less elements in the regions with smaller values of the potential gradient in order to decrease the computational effort.

After creating the mesh and using the *solver*, the values of the potentials in all nodes of the domain are calculated. Figure 6(b) illustrates the resulting equipotential lines after running the *solver* routine.

Since the magnetic field in the iron is very small and much greater in the air gap, the equipotential lines in this region are more concentrated, as expected.

2.2 Magnetic Induction Vector

After obtaining the equipotential lines, it is intended to obtain the magnetic field distribution throughout the core and the air gap, and, the determination of the magnetic induction vector in the air gap. To perform this step, the boundary conditions must be changed in order to solve the dual magnetic field problem: the homogeneous Neumann conditions are changed into Dirichlet boundary conditions and vice versa. The adopted mesh is the same as the mesh represented in Fig. 6(a).

In Fig. 7, the new boundary conditions are shown.

Running the *solver* routine with the boundary conditions shown in Fig. 7, the magnetic field lines will be obtained as the equipotential lines of the dual problem. If we want to obtain the magnetic induction lines instead of the magnetic field intensity lines, Eq. (5) must be solved replacing μ_r by $1/\mu_r$, which corresponds to Eq. (12) with $\vec{A}$ oriented in the axial direction and meeting $\vec{J} = 0$, imposing the dual boundary conditions of the problem described by Fig. 5, which is represented in Fig. 7.

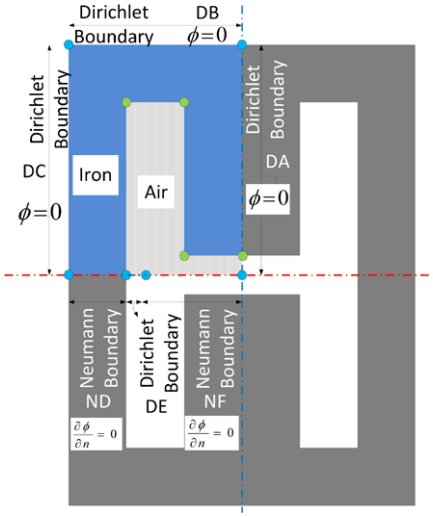

Fig. 7 Boundary conditions for the calculation of the magnetic induction vector

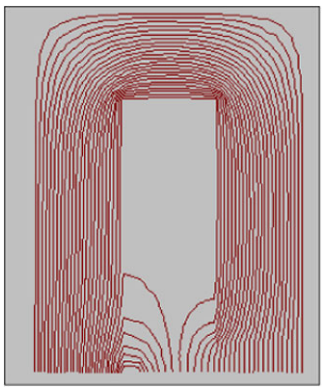

Fig. 8 Magnetic field lines

Thus, the magnetic induction field lines (Fig. 8) are obtained after running the *solver* for the boundary conditions of Fig. 7 replacing μ_r by $1/\mu_r$. Finally, the magnetic induction vector may be evaluated using (11) for the initial boundary value field problem indicated in Fig. 5.

Figure 9 illustrates the magnetic induction obtained along the core and air gap central axis when simulating the model with permanent magnets.

3 Core with Permanent Magnets and Superconductors

As can be seen in Fig. 9, the magnetic induction distribution obtained with the previous core does not fulfill the uniformity requirement.

To improve the uniformity of the magnetic induction, superconducting pieces are added to the initial core, as represented in Fig. 10.

Similar results to those in Figs. 6(a), 7, 8 and 9 are shown in Figs. 11, 12 and 13. As can be observed in Fig. 13, the

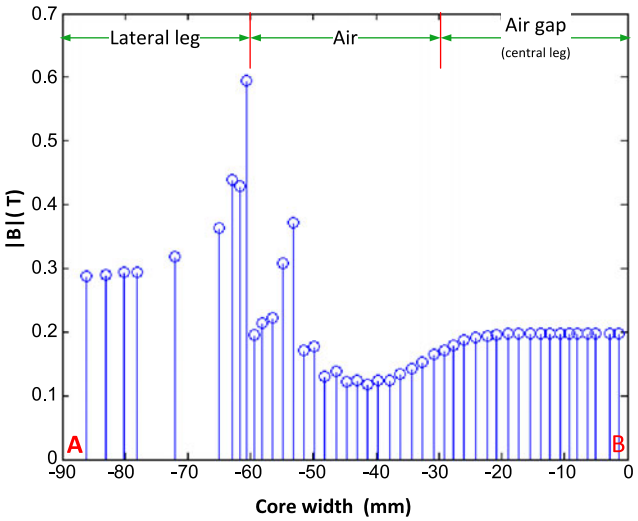

Fig. 9 Magnetic induction along the central axis of the core (AB—Fig. 3)

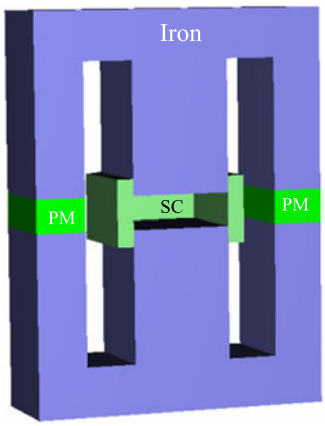

Fig. 10 Structure of the magnetic core with permanent magnets (PM) and superconductors (SC)

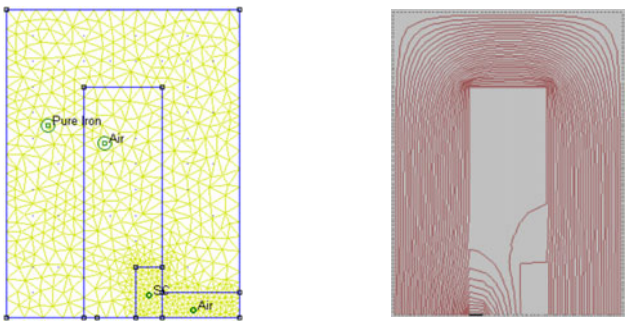

a) Mesh b) Magnetic field lines

Fig. 11 Finite-element mesh and magnetic field lines of the simulated section with superconductors

uniformity of the magnetic induction is reached when using the superconducting pieces.

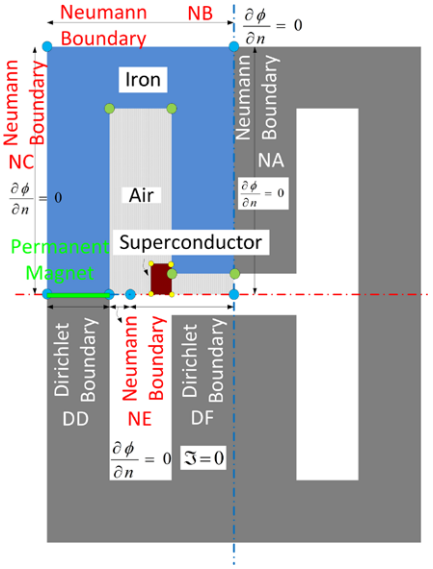

Fig. 12 Boundary conditions of the magnetic core with superconductors

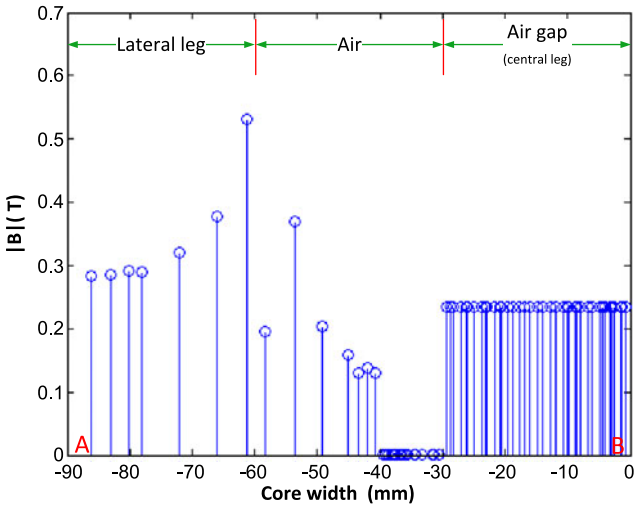

Fig. 13 Magnetic induction along the central axis of the core with superconductors (AB—Fig. 3)

4 Core with Coils and Superconductors

The real magnet instead of permanent magnets uses coils as represented in Fig. 14 without and with superconductors.

4.1 Calculation of the Potential

The vectorial formulation of the magnetic field problem considering the current in coils as the corresponding source can be obtained using the two-dimensional vectorial formulation [7]:

$$\nabla \times \frac{1}{\mu_r} \nabla \times \vec{A} = -\mu_0 \vec{J}. \tag{12}$$

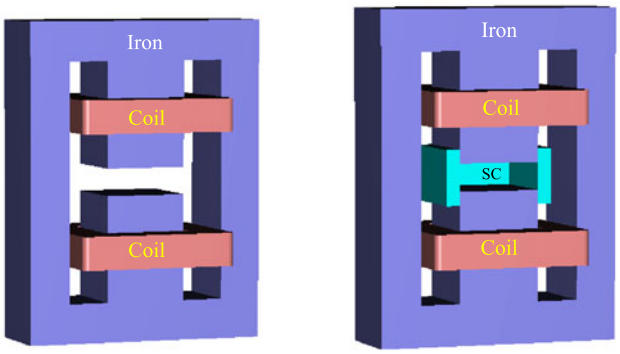

a)Without superconductors b) With superconductors

Fig. 14 Structures of the magnetic core with coils

The coils' total current is

$$\vec{I}_{\text{total}} = N\vec{I}, \tag{13}$$

where N is total the number of turns of the coils.

The total m.m.f. being equal to 1600 AT, the current density (J) is given by

$$\vec{J} = \frac{\vec{I}_{\text{total}}}{S}. \tag{14}$$

Here S is the cross section of the coil.

To obtain the magnetic induction in the air gap, it is known that

$$\vec{B} = \nabla \times \vec{A}. \tag{15}$$

For linear triangular finite elements, the potential is given by

$$\vec{A} = \sum_{i=1}^{3} A_i(a_i + b_i x + d_i y)\vec{u}_z. \tag{16}$$

The magnetic induction is then obtained by

$$\vec{B} = \left(\sum_{i=1}^{3} A_i d_i\right)\vec{u}_x - \left(\sum_{i=1}^{3} A_i b_i\right)\vec{u}_y. \tag{17}$$

Note that, for 2D field problems, the *solver* using Eqs. (12)–(17) is the same as for Eqs. (5)–(11).

In Fig. 15, the implemented models, with the appropriate media and boundary conditions, are shown.

Following the process referred previously when defining the boundaries, the resulting meshes are represented in Fig. 16.

After creating the mesh, running the *solver* and using the routine that allows calculating the magnetic induction field lines, the obtained magnetic field lines are represented in Fig. 17. Note that in this case the magnetic induction field lines are given by the equipotential lines directly.

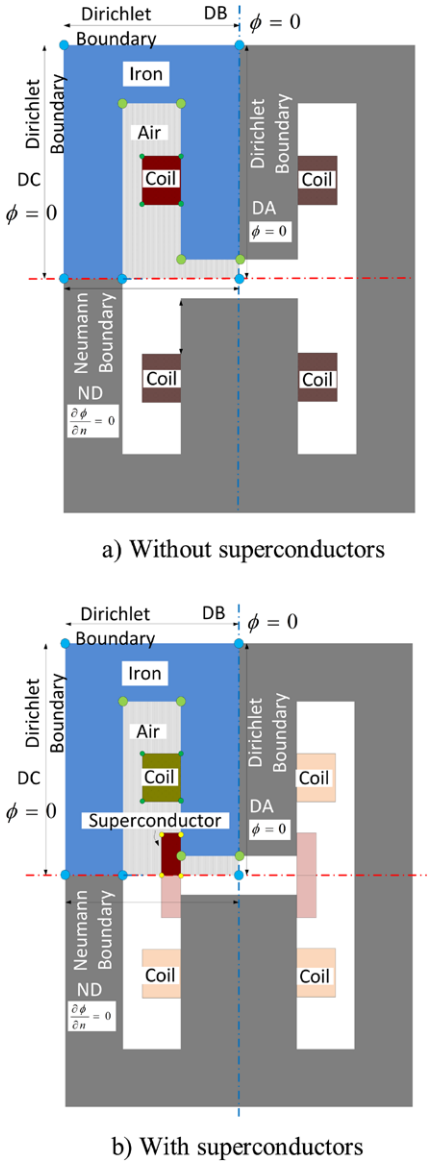

Fig. 15 Boundary conditions of the magnetic core with coils

In Fig. 18, the results of the magnetic induction vector for the core without and with superconductors are shown. These are key results knowing that the target application (FFC NMR) requires a magnet with high magnetic induction uniformity.

Results of Fig. 18(a) corresponds to a ration $\Delta B/B \approx 2.5$ %, translating a measure to the field uniformity, where B is an average value of the magnetic induction field along a central cross section with 4 cm^2 of area located in the air gap axis of symmetry and ΔB is the field variation along the same section. For the solution with superconducting pieces, the uniformity is, at least, 10 times better (Fig. 18(b)).

These results are in accordance with the ones presented in [11, 12], which were obtained for the same 4 cm^2 section of

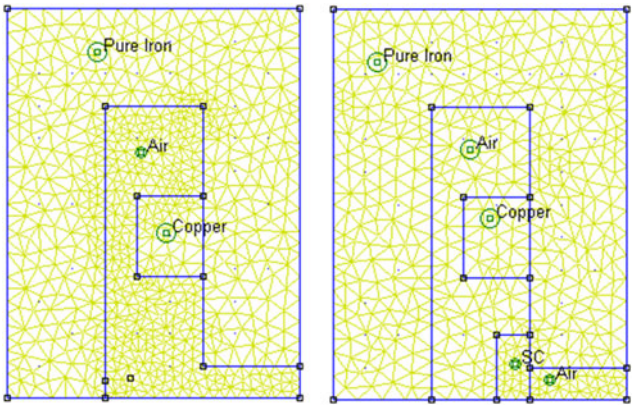

a) Without superconductors b) With superconductors

Fig. 16 Finite-element mesh of the simulated section with coils

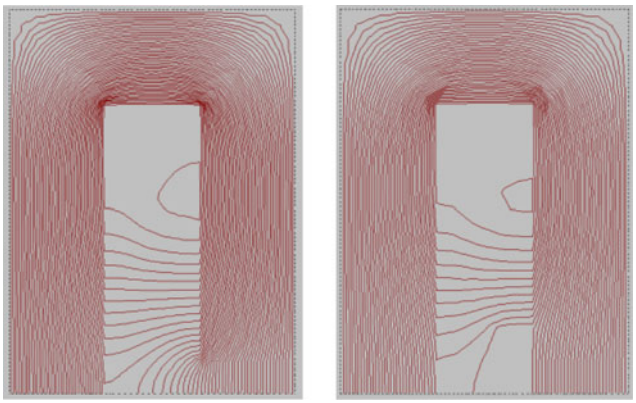

a) Without superconductors b) With superconductors

Fig. 17 Magnetic field lines with coils

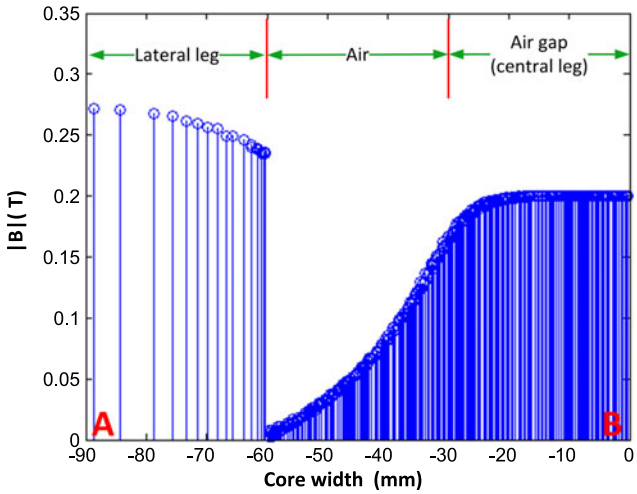

a) Without superconductors

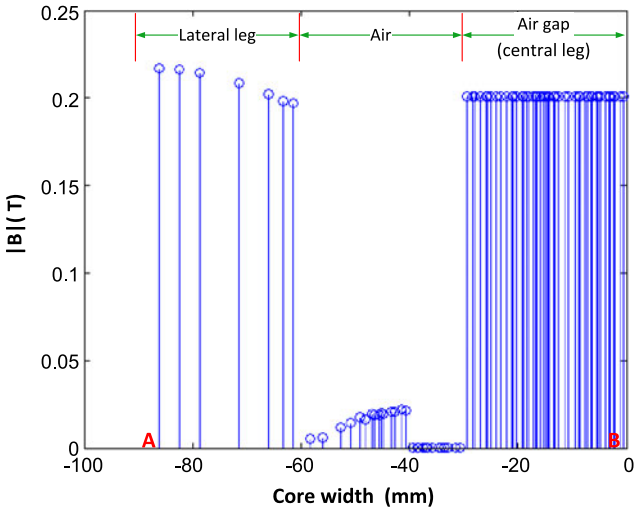

b) With superconductors

Fig. 18 Magnetic induction along the central axis of the core with coils (AB—Fig. 3)

the air gap central layer using a commercial finite-element method program [4].

In order to validate the results obtained with the implemented routines, taking advantage of the capabilities of the referred commercial finite-element program, the core with coils generating the same m.m.f., without and with superconductors, was simulated.

The results of this simulation, shown in Fig. 19, agree, with deviations less than 2 %, to those obtained by running the *solver* implemented for this work.

In Fig. 20 an image of the real magnet including superconducting pieces is shown.

5 Conclusion

In this paper, the simulation results of a magnetic core with different configurations are shown. These results are obtained with routines implemented using the scalar potential and vector potential approaches.

The main objectives of this work are to determine the value of the magnetic induction in air gap of a magnetic core, and to observe the magnetic field lines around the model.

Since the model under study has a symmetrical configuration, only one quarter (1/4) of the model is simulated by imposing the appropriate boundary conditions, reducing the computational effort, but keeping the final results valid if extended to the whole model.

For the different configurations of the magnet, the magnetic field lines in the magnetic core and in the air gap are observed, and the magnetic induction vector in the central axis of the air gap is computed. In all simulations, the target value of the vector of magnetic induction in the central part of the air gap is approximately 0.2 T. The introduction of superconductors has a significant improvement in the uniformity of the field along the central axis of the air gap.

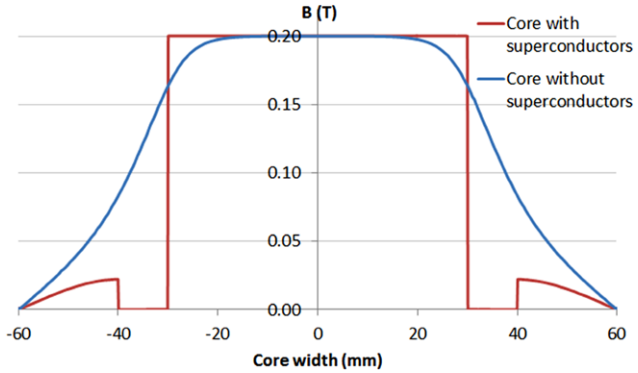

Fig. 19 Flux density along the central axis of the magnetic core (excluding the external legs)

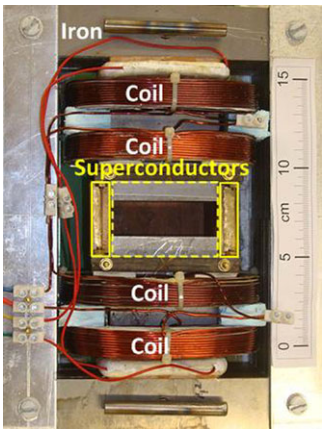

Fig. 20 Real magnet including superconducting pieces

In conclusion, comparing the above results and those presented in the literature, the developed *solver* constitutes a valid and useful tool in order to design FFC NMR magnets. Furthermore, the described approach allows for modeling the magnetic system, taking into account the specificities of materials and sources.

Acknowledgements The authors thank the "Center for Innovation in Electrical and Energy Engineering" (CIEEE) of the IST/TU Lisbon and the "Fundação para a Ciência e a Tecnologia" (FCT) for financial support of this work.

References

1. Noack, F.: NMR field-cycling spectroscopy: principles and applications. Prog. Nucl. Magn. Reson. Spectrosc. **18**, 171–276 (1986)
2. Abragam, A.: The Principles of Nuclear Magnetism. Oxford University Press, London (1978)
3. Sousa, D.M.: Desenvolvimento de um espectrómetro de ressonância magnética nuclear de campo cíclico rápido. Ph.D. thesis, Instituto Superior Técnico, Lisbon (2003)
4. FEMM 3.3. www.femm.info/. Accessed 16 June 2011
5. Meissner, W., Oschsenfeld, R.: Ein neuer Effect bei Eintritt der Supraleitfahigkeit. Naturwissenschaften **21**(44), 787–788 (1933)
6. Bean, C.P.: Magnetization of high-field superconductors. Rev. Mod. Phys. **36**, 31–39 (1964)
7. Cermak, R., et al.: Overview of magnetic levitation principles and their application in Maglev trains. Adv. Eng. **2**, 19–28 (2008)
8. Binns, K.J., Lawrenson, P.J., Trowbridge, C.W.: The Analytical and Numerical Solution of Electric and Magnetic Fields. Wiley, New York (1992)
9. Sardanha, A.U.: Aplicacion del método de elementos finitos al perfeccionamiento de pinzas amperimétricas. Thesis Doctoral, Departamento de Ingenharía Eléctrica, Universidade de Zaragoza (2007)
10. Bastos, J.P.A., Sadowski, N.: Electromagnetic Modeling by Finite Element Methods. Marcel Dekker, Inc., New York (2003)
11. Roque, A., Sousa, D.M., Margato, E., Maia, J., Marques, G.D.: Characterization of the fringing window of a magnetic core. In: IEEE EUROCON 2011—International Conference on Computer as a Tool, Lisbon, Portugal (2011)
12. Roque, A., Sousa, D.M., Margato, E., Maia, J., Marques, G.D.: Fringing window of a magnet with high flux density uniformity-magnetic core with and without superconductors. In: IEEE 2011 International Conference on Applied Superconductivity and Electromagnetic Devices (ASEMD2011), Sydney, Australia (2011)